DOI: 10.1002/ente.201700777

Direct Alcohol-Fueled Low-Temperature Solid Oxide Fuel Cells: A Review

Byung Chan Yang[+],[a] Junmo Koo[+],[b] Jeong Woo Shin,[a] Dohyun Go,[a] Joon Hyung Shim,*[b] and Jihwan An*[a]

Low-temperature solid oxide fuel cells (LT-SOFCs, operating temperature $\leq 600\,^{\circ}C$) are advantageous in potential applicability, affordability, and durability compared to conventional SOFCs (operating temperature: 800–1000 °C). Direct operation of LT-SOFCs on liquid alcohol fuels can further improve their portability as well as accessibility to the fuel. In this review, we overview the results of LT-SOFCs directly fueled by liquid alcohols that operate at 600 °C and below. Fundamentals regarding operation principles, losses, as well as reactions associated with liquid alcohol-fueled LT-SOFCs are presented. The materials, structures, and fabrication processes of cell components, namely anode, electrolyte, and cathode, are mainly reviewed. The electrochemical performances of alcohol-fueled LT-SOFCs are also summarized and compared with those of H_2-fueled LT-SOFCs.

1. Introduction

Solid oxide fuel cells (SOFCs) have drawn much attention as promising next-generation energy conversion devices due to their advantages such as high energy-conversion efficiency (up to 80 % in combined heat and power (CHP) mode operation), environmental friendliness (no CO_2 emission when operated with H_2 fuel), and fuel flexibility (hydrocarbon fuels as well as H_2).[1–4] While conventional SOFCs operate at high temperatures (usually above 800 °C) due to temperature-dependent nature of the individual processes of cell operation, the high operating temperature often causes practical problems such as thermal insulation, performance degradation due to high temperature oxidation, corrosion and phase transition of the components, and thermal expansion mismatch between the components. The application of SOFCs have thus been largely limited to stationary applications.[5,6] Therefore, SOFCs operating at a low temperature range ($\leq 600\,^{\circ}C$), namely low-temperature SOFCs (LT-SOFCs), have recently been widely researched to overcome the issues stemming from high operating temperatures either with microfabrication techniques[4,5,7–18] or conventional fabrication techniques.[19–24] Reduction in operating temperature allows the use of cheaper interconnects and sealing materials and accelerates the start-up and shut-down of the cells, thus increasing the affordability and broadening the applicability of SOFCs from conventional stationary applications to portable applications.[14]

Fuel is another important issue for the applicability of SOFCs; while the wide use of hydrogen is restricted by low availability of cost-effective storage technology and distribution infrastructure, liquid alcohol fuels such as methanol (MeOH) or ethanol (EtOH) are largely free of storage and distribution issues without the need for new infrastructures.[25] A comparison of properties of H_2, MeOH, and EtOH is presented in Table 1. MeOH and EtOH are considered as both a hydrogen source and a direct fuel. The use of MeOH and EtOH for SOFCs has not been fully explored, mainly because SOFCs are usually intended for stationary applications.[26] However, for small-scale portable applications, MeOH is an attractive fuel candidate because it is a liquid with high volumetric energy density (15.9 MJL^{-1} at Standard Temperature and Pressure (STP) condition), especially compared to that of hydrogen gas (0.01 MJL^{-1} at STP), which makes it easier to store and transport. Moreover, the impurity content that poisons the anode is low; the amount of carbon predicted at equilibrium is significantly lower than the carbon content observed for EtOH, liquefied petroleum gas (LPG), gasoline, or diesel.[27,28] Therefore, many researches on MeOH-fueled LT-SOFCs have been reported. Compared to MeOH, the utilization of EtOH as a SOFC fuel has been considered relatively recently. While EtOH shares advantages

Table 1. Properties of hydrogen, MeOH, and EtOH fuels for fuel cells. Reproduced with permission.[25] Copyright 2015, Elsevier.

Property	Hydrogen	MeOH	EtOH
Formula	H_2	CH_3OH	C_2H_5OH
$-\Delta G^{\circ}$ ($KJ\,mol^{-1}$)	237	702	1325
$-\Delta H$ ($KJ\,mol^{-1}$)	286	726	1367
Energy density, LHV ($kWh\,kg^{-1}$)	33	6.09	8.00
Energy density, LHV ($kWh\,L^{-1}$)	2.96×10^{-3}	4.80	6.32
E^{0}_{cell} (V)	1.23	1.21	1.14
Energy stored ($Ah\,kg^{-1}$)	26,802	3350	2330
Energy stored ($Ah\,L^{-1}$)	2.40	2653	1841

[a] B. C. Yang,[+] J. W. Shin, D. Go, Prof. J. An
Department of Manufacturing Systems and Design Engineering
Seoul National University of Science and Technology (SeoulTech)
232 Gongneung-ro, Nowon-gu, Seoul 139-743, Republic of Korea
E-mail: jihwanan@seoultech.ac.kr

[b] J. Koo,[+] Prof. J. H. Shim
Department of Mechanical Engineering
Korea University
Anam-dong, Seongbuk-gu, Seoul 136-713, Republic of Korea
E-mail: shimm@korea.ac.kr

[+] These authors contributed equally

with MeOH, such as high volumetric energy density (18.4 MJL^{-1}), cleanliness, and portability, it is difficult to oxidize EtOH compared to H_2 or MeOH. The reforming of EtOH is more challenging than that of MeOH due to severe coking. The direct utilization of EtOH for LT-SOFCs has been reported in several literatures.[29,30] The use of glycerol as a fuel for LT-SOFCs has also been reported.[4]

A practical problem in LT-SOFCs operating directly on liquid alcohol fuels, however, is their relatively low performance compared to those based on H_2 fuel due to more complex electrochemical processes and carbon coking, which can significantly increase the activation loss at anode, and therefore lower the performance. Moreover, the power densities and lifetimes of alcohol-based SOFCs are much below the requirements for the commercialization of the technology.[25] Therefore, the selection of materials and structures for LT-SOFC components, i.e., anode, electrolyte, and cathode, as well as the optimal combination of these are crucial to meeting the requirement for commercialization.

In this article, we review the results of LT-SOFCs based on liquid alcohol fuels directly that operate at 600 °C and below. Fundamentals that are closely relevant with the performance of alcohol-fueled LT-SOFCs such as fuel cell losses in low-temperature operation as well as anode kinetics based on MeOH and EtOH fuels are first discussed. We mainly focus on materials, structures, and fabrication processes of the cell components: anode, electrolyte, and cathode. Lastly, the electrochemical performances of alcohol-fueled LT-SOFCs are reviewed and compared to those of H_2-fueled LT-SOFCs.

2. Fundamentals of Alcohol-Fueled LT-SOFC

2.1. SOFC Fundamentals

The cell voltage of SOFC (V) can be described as a function of open circuit voltage (OCV, V_{oc}) and losses including activation loss at anode ($\eta_{act,anode}$) and cathode ($\eta_{act,cathode}$), ohmic loss (η_{ohmic}), and concentration loss (η_{conc}), as shown in the following equation:[31]

$$V = V_{oc} - \eta_{act,anode} - \eta_{act,cathode} - \eta_{ohmic} - \eta_{conc}$$

In H_2-fueled SOFCs, concentration loss that arises from mass transport of fuel or oxidant molecules is usually ignored. In alcohol-fueled SOFCs, however, concentration loss sometimes causes non-negligible decrease in cell performance, especially when EtOH fuel is used due to its high molecular weight. Assuming that the contribution of concentration loss to the total loss is not significant, and therefore negligible, SOFCs with high cell voltage as well as high power density (i.e., maximum power density of $>1\ W\,cm^{-2}$)[14] can be achieved by minimizing the ohmic and activation losses.

Jihwan An is an Assistant Professor in the Department of Manufacturing Systems and Design Engineering at Seoul National University of Science and Technology (SeoulTech), Korea, since 2014. Before joining SeoulTech, he worked as a research associate and a lecturer in the Department of Mechanical Engineering at Stanford University. He received his MS and PhD degrees in Mechanical Engineering from Stanford University in 2009 and 2013, respectively, and BS degree in Mechanical and Aerospace Engineering from Seoul National University in 2007. His current research interests include nanoscale phenomena in solid oxide fuel cells as well as thin film processes.

Joon Hyung Shim is an Associate Professor of Mechanical Engineering and a Director of the Renewable Energy Laboratory (RES-Lab) at Korea University (KU). Before joining KU as a faculty, he was a postdoctoral researcher at National Renewable Energy Laboratory (NREL) and a full-time lecturer of Mechanical Engineering at Stanford University. He received his B.S. degree in Mechanical and Aerospace Engineering from Seoul National University in 2002, and M.S. and Ph.D. degrees in Mechanical Engineering from Stanford University in 2004 and 2009, respectively.

Byung Chan Yang received his B.S. degree in Manufacturing Systems and Design Engineering Program in 2017 from Seoul National University of Science and Technology (SeoulTech), Seoul, Republic of Korea. He is currently pursuing his M.S. degree in SeoulTech (Advisor: Prof. Jihwan An). His research interests include the applications of thin film processes to low-temperature solid oxide fuel cells, and the development of novel nanostructured components for thin film solid oxide fuel cells.

Junmo Koo received his B.S. in Mechanical Engineering in 2014 from the Korea University (Seoul, Republic of Korea) and is currently pursuing Ph.D. in Mechanical Engineering from Korea University. His research interests are in the area of nanoparticle and thin film synthesis by deposition techniques including ALD, CVD, and sputtering, and their application in polymer electrolyte membrane fuel cells and solid oxide fuel cells.

While the ohmic and activation losses in SOFCs operating at high temperatures (>800 °C) are relatively small (i.e., total area specific resistance (ASR) value of <0.45 Ω cm^2),[14] the losses significantly increase in the operation condition of LT-SOFCs due to the thermally activated nature of the relevant processes: ohmic loss that mainly arises from ionic transport through electrolyte and activation loss that stems from the electrochemical processes at electrodes sharply increase at low temperatures because of the exponential dependence of ionic conductivity and charge transfer reaction rate on temperature, respectively. The activation loss at cathode is more dominant than that at anode because of sluggish oxygen reduction (E_a >1 eV) in H_2-O_2 LT-SOFCs. Therefore, in H_2-fueled LT-SOFCs, the engineering of electrolyte and cathode have been crucial. Recent reviews on LT-SOFCs can be found elsewhere.[14,31]

However, in direct alcohol-fueled LT-SOFCs, the activation loss at anode is not negligible, or sometimes dominant, due to the much more complex oxidation process of alcohol molecules (MeOH and EtOH) compared to that of H_2.[25] Schematic illustrations of alcohol-fueled LT-SOFCs during operation are shown in Figure 1. Carbon formation is also a

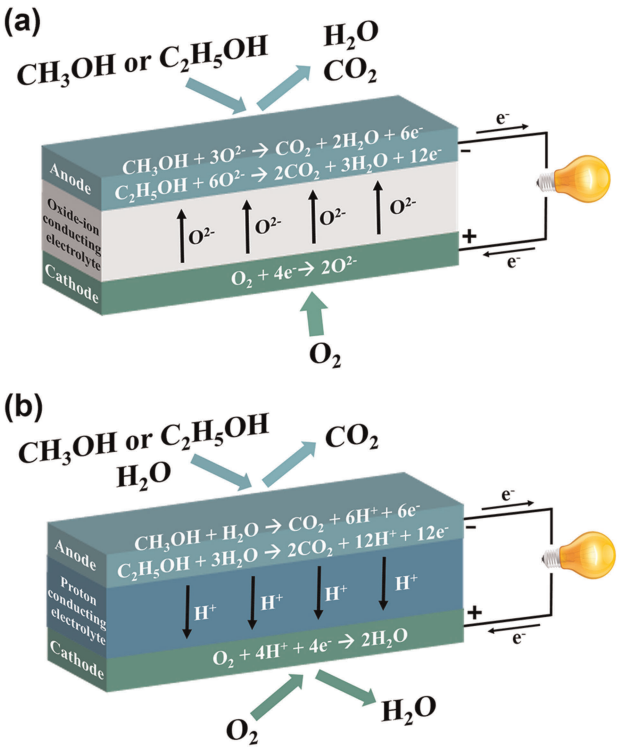

Figure 1. Schematic illustrations of alcohol-fueled SOFCs during their operations: (a) with oxide-ion conducting electrolytes and (b) with proton conducting electrolytes

significant cause that renders the anode reaction unstable.[26] Particularly at lower temperatures (≤600 °C) compared to the operating temperature of conventional SOFCs, carbon (as graphite, which is the lowest energy polymorph of carbon) can be more thermodynamically favored than CO or H_2 are, leading to a lower equilibrium potential (1.04 V at 600 °C vs. 1.13 V at 900 °C for MeOH; 1.05 V at 600 °C vs. 1.15 V at 900 °C for EtOH) in the pyrolysis of MeOH and EtOH (Figure 2).[32] The kinetics at SOFC anode with MeOH and EtOH fuels are further discussed in the following section.

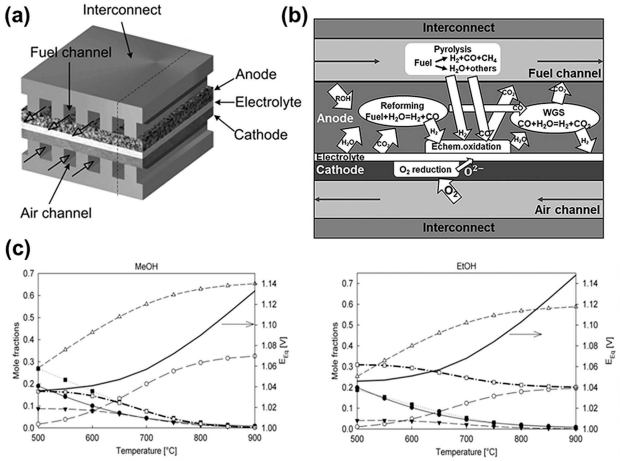

Figure 2. (a) Schematics of a planar SOFC cross section, (b) processes involved in the direct utilization of hydrocarbons in a SOFC (WGS is the water-gas shift reaction), and (c) equilibrium compositions (symbols) and potentials (solid lines) as a function of temperature for MeOH and EtOH pyrolysis. The species are (●) CH_4, (○) CO, (▼) CO_2, (△) H_2, (■) H_2O, and (□) C (graphite). Reproduced with permission.[26] Copyright 2009, MDPI.

2.2. Fuels and Anode Reactions

Figure 1 shows the schematic illustrations of electrochemical reactions involved in direct alcohol-fueled SOFCs during their operations with MeOH and EtOH fuels with different kinds of electrolytes (oxide-ion-conducting and proton-conducting electrolytes), including anode and cathode reactions as well as ionic transport through electrolytes. While more detailed individual reaction pathways are discussed both in this review and in other literatures,[26,33–46] it should be noted that the location where net water formation occurs could be altered depending on the type of electrolyte: at anode with oxide-ion-conducting electrolytes and at cathode with proton-conducting electrolytes. The water molecules produced in such a way may participate in subsequent reactions. Also the water molecules participate as reactants in anodic reactions in the cells with proton-conducting electrolytes.[25] The following paragraph about anodic reactions is assuming the use of oxide-ion conducting electrolyte, which is the most widely used type of electrolyte for SOFCs.

Detailed description of possible reaction pathways for alcohol fuels directly provided to the anode side has been presented by Cimenti et al. (Figures 2(a) and 2(b)).[26] First, the fuel undergoes pyrolysis, forming products such as H_2 and CO. The fuel molecules together with pyrolysis products can decompose on the anode surface, i.e., catalytic decomposi-

tion. Afterwards, the products of pyrolysis and catalytic decomposition as well as undecomposed fuel molecules can undergo partial or full oxidation by reacting with oxygen ions that transported through the electrolyte, i.e., electrochemical oxidation, forming H_2O and CO_2. H_2O and CO_2 can lead to other reactions, which reform the fuel molecules into H_2 (steam reforming) and CO (dry reforming). H_2O may react with CO from decomposition and reforming, releasing H_2 and CO_2 (water-gas shift). In the meantime, carbon formation and removal (coking) can also occur. The processes discussed above can depend on various conditions such as temperature, pressure, flow condition, and catalytic properties of the anode, as well as the current density.

The specific reaction pathways at anode with MeOH fuel can include the following:[33]

$$CH_3OH + H_2O = CO_2 + 3H_2 \text{ (MeOH steam reforming)}$$

$$CH_3OH = CO + 2H_2 \text{ (MeOH decomposition)}$$

$$CH_3OH + 0.5O_2 = CO_2 + 2H_2 \text{ (partial oxidation)}$$

Here, hydrogen can be further generated by the water–gas shift reaction as follows:

$$CO + H_2O = CO_2 + H_2$$

In addition, methanation reactions are also known to occur at a low steam-to-carbon ratio:

$$CO + 3H_2 = CH_4 + H_2O$$

$$CO_2 + 4H_2 = CH_4 + 2H_2O$$

Carbon coking may occur via disproportionation of CO (Boudouard reaction):

$$2CO = C + CO_2,$$

and direct electrochemical oxidation of MeOH fuel can also occur by accepting oxide ions at the anode-electrolyte interface:

$$CH_3OH + 3O^{2-} = CO_2 + 2H_2O + 6e^-$$

where the following intermediate reactions may occur:[34]

$$CH_3OH + 2O^{2-} = HCOOH + H_2O + 4e^-$$

$$HCOOH + O^{2-} = CO_2 + H_2O + 2e^-$$

EtOH may have much more complex reaction pathways at anode including thermal decomposition and steam reforming, i.e., $C_2H_5OH + H_2O = 2CO + 4H_2$, in the temperature range of 400–600 °C,[35–38] resulting in H_2 and CO-rich fragments that can be efficiently used as fuel as a consequence of electrochemical oxidation at the anodes of LT-SOFCs:[39,40]

$$H_2 + O^{2-} = H_2O + 2e^-$$

$$CO + O^{2-} = CO_2 + 2e^-$$

Alternately, a gradual internal reforming pathway based on steam reforming as well as hydrogen electrochemical oxidation has been proposed.[41,42] In this reaction, water released by the electrochemical oxidation of hydrogen at the anode is used for the steam reforming of EtOH in a catalytic layer deposited over the anode:[42–45]

Direct electrochemical oxidation of EtOH fuel can also occur

$$C_2H_5OH + 3H_2O = 2CO_2 + 6H_2$$

$$H_2 + O^{2-} = H_2O + 2e^-$$

by accepting oxygen ions at the anode-electrolyte interface:[46]

$$CH_5OH + 3O^{2-} = 3H_2 + 2CO_2 + 6e^-$$

More detailed descriptions on electrolyte and cathode reactions associated with LT-SOFCs can also be found in other recent review articles.[14,31,47]

3. Membrane Designs and Materials

The general membrane design of a LT-SOFC is composed of three components: anode, electrolyte, and cathode. Anode and cathode are fabricated with porous structures to maximize the reaction area for activation processes, and therefore reduce the activation loss at the electrode. Catalytically active materials for MeOH/EtOH oxidation reactions are used as anodes: non-noble metal (e.g., Ni, Cu, or Ni–Cu alloys mixed with electrolyte materials) or noble metal (e.g., Pt, Pd, Ag, or Pt–Ru alloys) based materials. Catalytically active materials for oxygen reduction reaction are used as cathodes: oxide-based (e.g., $La_{1-x}Sr_xCoO_{3-\delta}$ (LSC), $La_{1-x}Sr_xCo_yFe_{1-y}O_{3-\delta}$ (LSCF), or $Ba_{1-x}Sr_xCo_yFe_{1-y}O_{3-\delta}$ (BSCF)) or noble metal (e.g., Pt and Ag) based materials). Electrolytes are composed of dense ion-conducting oxides such as oxide-ion conducting (e.g., ytrria-stabilized zirconia (YSZ), gadolinia-doped ceria (GDC), or samaria-doped ceria (SDC)) or proton conducting (e.g., yttria-doped barium zirconate (BYZ)) ceramics. Membrane structures and materials, as well as performances of direct alcohol-fueled LT-SOFCs are summarized in Table 2.

3.1. Anode

3.1.1. Non-Noble Metal Based

Studies on anodes can be categorized according to the type of materials: non-noble-metal-based and noble-metal-based results. These studies aim to improve the performance in three main aspects: suppressing coking, enhancing alcohol oxidation kinetics, and improving chemical and mechanical stability (Table 2). Among the non-noble metals, Ni is the most

Table 2. Summary of structures, materials, and performances of LT-SOFCs based on direct alcohol fuels. Reports are categorized according to the main theme (anode, electrolyte, cathode). Main focus in anode studies (coking, kinetics, stability) are also presented for results on anode

Main focus in anode studies			Anode	Electrolyte	Cathode	Maximum power density [$mWcm^{-2}$]	Fuel	Main points	Ref
Coking	Kinetics	Stability	Reports mainly on anode engineering						
			Ni (150 μm)			78 at 500 °C 88 at 500 °C 98 at 500 °C	2:1 Methanol/water 4:1 Methanol/water 4:1 Ethanol/water		
O	–	–	Cu-based (150 μm)			31 at 500 °C 40 at 500 °C 51 at 500 °C	2:1 Methanol/water 4:1 Methanol/water 4:1 Ethanol/water		[54]
				$BaCe_{0.48}Zr_{0.4}Yb_{0.1}Co_{0.02}O_{3-\delta}$ (BCZYbCo) (30–35 μm)	$BaCe_{0.48}Zr_{0.4}Yb_{0.1}Co_{0.02}O_{3-\delta}$ (BCZYbCo) / $La_{1-x}Sr_xCoO_{3-\delta}$ (LSC) (25 μm)			Alloying Ni with Cu to limit carbon formation at the anode	
			Ni–Cu(150 μm)			22 at 500 °C 25 at 500 °C 17 at 500 °C	2:1 Methanol/water 4:1 Methanol/water 4:1 Ethanol/water		
O	O	–	$Li_{0.2}Ni_{0.7}Cu_{0.1}O$-Samarium doped ceria-sodium carbonate (NSDC)	Samarium doped ceria-sodium carbonate (NSDC)	$Li_{0.2}Ni_{0.7}Cu_{0.1}O$- Samarium doped ceria-sodium carbonate (NSDC)	150 at 580 °C 215 at 580 °C	Bio-Ethanol Glycerol	Increased performance due to small dipole moment response of bio ethanol	[35]
–	O	–	Ni–Cu-ZnO(50%) composite with electrolyte(50%) (0.4 mm)	Nanocomposite of samaria-doped ceria (SDC) and Na_2CO_3 (0.3 mm)	Ni–Cu-ZnO composite with electrolyte (0.3 mm)	400 at 480 °C 514 at 520 °C 584 at 570 °C	Bio-Ethanol	Functional nanocomposite electrodes that is effective for liquid based fuel cells	[46]
O	–	O	NiO + $(Y_2O_3)_{0.1}(ZrO_2)_{0.9}$ (YSZ) with $NiAl_2O_3$ catalyst (800 μm)	$(Y_2O_3)_{0.1}(ZrO_2)_{0.9}$ (YSZ) (10 μm)	$Ba_{1-x}Sr_xCo_yFe_{1-y}O_{3-\delta}$ (BSCF)/ $Sm_{0.5}Sr_{0.25}CoO_{3-\delta}$ (SSC) + $Sm_{0.2}Ce_{0.8}O_2$ (SDC) (25 μm)	300 at 600 °C	Ethanol/pyridine	Addition Pyridine to ethanol fuel gas suppressed coke formation and improved stability	[48]
Non-noble metal based	O	O	Ru coated Ni (45–53 nm)	$Cd_{0.1}Ce_{0.9}O_{2-\delta}$ (GDC) (350 μm)	Pt (~150 nm)	0.5 at 300 °C	Methanol	ALD Ru islands improving surface kinetics for methanol oxidation and thermal stability with less Ni coarsening and reducing the content of adsorbed carbon on the anode	[49]

Table 2. continued

Main focus in anode studies			Anode	Electrolyte	Cathode	Maximum power density [mWcm^{-2}]	Fuel	Main points	Ref
Coking	Kinetics	Stability	Reports mainly on anode engineering						
O	O	–	Ni + Yttria stabilzed zirconia (YSZ) (anode support : 1 mm) (anode interlayer : ~ 20 µm) Cu–$Ce_{0.9}Gd_{0.1}O_{1.95}$ (GDC) (30–50 µm) Cu–Ceria (30–40 µm)	Yttria stabilzed zirconia (YSZ) (~10 µm)	$La_{0.8}Sr_{0.2}MnO_{3-\delta}$ (LSM) (~80 µm)	200 at 550 °C	Methanol	Low activation and concentration polarization for methanol with small molecular weight	[53]
O	–	O	NiO/ Samaria-doped ceria (SDC)	$Ce_{0.9}Gd_{0.1}O_{1.95}$ (GDC) (0.7 mm) Samaria-doped ceria (SDC) (24 µm)	$La_{0.6}Sr_{0.4}Co_{0.2}Fe_{0.8}O_{3-\delta}$ (LSCF) (15 µm) $Sm_{0.5}Sr_{0.25}CoO_3$ (SSC) /Samaria-doped ceria (SDC)	- 9 at 600 °C 223 at 550 °C 430 at 600 °C	Methanol/ water steam Methanol	Catalytic activity of methanol decomposition was lost due to sintering at 600 °C (Cu–Ceria). Direct Methanol fueled SOFC shows long term stability without coking	[33] [55]
O	–	O	Ni + $Sm_{0.2}Ce_{0.8}O_{1.9}$ (SDC) (50 µm)	$Sm_{0.2}Ce_{0.8}O_{1.9}$ (SDC) (360 µm)	$Ba_{1-x}Sr_xCo_yFe_{1-y}O_{3-\delta}$ (BSCF) + $Sm_{0.2}Ce_{0.8}O_{1.9}$ (SDC) (30 µm)	500 at 600 °C	Methanol flame	No carbon deposition with methanol flame vs. severe carbon deposition with ethanol flame	[56]
–	O	–	Ni - $Ce_{0.85}Sm_{0.15}O_{1.925}$ (SDC) (anode support: 0.6 mm) (active anode layer: ~12 µm)	$Ce_{0.85}Sm_{0.15}O_{1.925}$ (SDC) (~6 µm)	$Ce_{0.85}Sm_{0.15}O_{1.925}$ (SDC) -$La_{0.6}Sr_{0.4}Co_{0.2}Fe_{0.8}O_{3-\delta}$ (LSCF)	110 at 450 °C 260 at 500 °C 520 at 550 °C 820 at 600 °C	Methanol	More active sites for fuel oxidation reaction due to thin electrolyte with uniform pores	[57]
–	–	–	C–MO-SDC (C = activation carbon / carbon black, M = Cu, Ni, and Co, SDC = $Ce_{0.9}Sm_{0.1}O_{1.95}$)	Ceria-salt composite(CSC) (1 mm)	-	250 at 560 °C	Methanol	Improvement of electronic conductivity of anode by adding carbon having high electronic conductivity and oxidation-resistant property	[58]
-	O	-	Pd-added NiO - Yttria stabilzed zirconia (YSZ) (1 mm)	$Ce_{0.9}Gd_{0.1}O_{1.95}$ (GDC) (5 µm)	$La_{0.8}Sr_{0.4}Co_{0.2}Fe_{0.8}O_{3-\delta}$ (LSCF)	32 at 550 °C 65 at 600 °C 15 at 550 °C 40 at 600 °C	Methanol (reformed CH_3OH) Methanol/ H_2O	Pd facilitating the internal reforming /decomposition of methanol at the anode	[61]
–	O	–	NiO + $BaZr_{0.1}Ce_{0.7}Y_{0.1}Yb_{0.2}O_{3-\delta}$ (BZCYYb)	$Sm_{0.2}Ce_{0.8}O_{1.9}$ (SDC) (~20 µm)	$Ba_{1-x}Sr_xCo_yFe_{1-y}O_{3-\delta}$ (BSCF) (15 µm)	519 at 600 °C	Ethanol	BZCYYb has good oxygen ion conductivity, small particle size, high water storage capability and good coking resistance	[62]
O	O	–	NiO + $(Y_2O_3)_{0.1}(ZrO_2)_{0.9}$ (YSZ) with Ni + $Ce_{0.8}Zr_{0.2}O_2$ catalyst layer	$(Y_2O_3)_{0.1}(ZrO_2)_{0.9}$ (YSZ) (10 µm)	$Ba_{1-x}Sr_xCo_yFe_{1-y}O_{3-\delta}$ (BSCF) + $Sm_{0.5}Sr_{0.25}CoO_{3-\delta}$ (SSC)	179 at 550 °C 324 at 600 °C	Ethanol/ O_2	Improvement of hydrogen selectivity and coking resistance due to Ni + $Ce_{0.8}Zr_{0.2}O_2$ catalyst layer	[65]
O	O	O	NiO + $(Y_2O_3)_{0.1}(ZrO_2)_{0.9}$ (YSZ) with Ni-$Ce_{0.8}Zr_{0.2}O_2$ catalyst layer	$(Y_2O_3)_{0.1}(ZrO_2)_{0.9}$ (YSZ)	$Ba_{1-x}Sr_xCo_yFe_{1-y}O_{3-\delta}$ (BSCF)	162 at 600 °C 74 at 550 °C	Ethanol/ water steam gas	Good coking resistance due to the strong interaction between Ni and $Ce_{0.8}Zr_{0.2}O_2$ also it has good catalytic activity for EtOH conversion to hydrogen	[66]

Table 2. continued

	Main focus in anode studies			Anode	Electrolyte	Cathode	Maximum power density [mWcm^{-2}]	Fuel	Main points	Ref
	Coking	Kinetics	Stability	Reports mainly on anode engineering						
Noble metal based	–	O	–	$Pt_{0.4}Ru_{0.6}$(80 nm)	8 mol% yttria stabilzed zirconia (YSZ) (100 μm)	Pt(60 nm)	0.0015 at 250 °C 0.0073 at 300 °C 0.071 at 350 °C	Methanol	Lower catalytic activity of Pt–Ru alloy anode compared to Pt anode	[70]
	–	O	O	Ru-coated(< 20 nm) Pt(150 nm)	$Gd_{0.1}Ce_{0.9}O_{2-\delta}$ (350 μm)	Pt(150 nm)	5.5 at 400 °C 8.5 at 450 °C	Methanol	Prevention of coarsening of Pt cluster due to passivated layer by Ru oxidation	[71]
	O	O	O	Ru-coated(< 10 nm) Pt(150 nm)	$Gd_{0.1}Ce_{0.9}O_{2-\delta}$ (350 μm)	Pt	13 at 500 °C 4 at 550 °C	Ethanol 3.5 kPa: 7.5 kPa Ethanol/water	Increased surface kinetics and reduced anode impedance by ALD Ru coating without coking	[72]
	–	O	–	Pt	Yttria stabilzed zirconia (YSZ)	Pt	3 at 550 °C	5 kPa: 7.5 kPa Ethanol/water	Ag anode shows inferior performance compared to Pt anode	[74]
				Ag		Ag	2 at 550 °C	5 kPa: 7.5 kPa Ethanol/water		
	O	–	–	Pd	Y-$BaZrO_3$ (BYZ) (130 nm)	Pt	15.3 at 400 °C	Ethanol vapor	Increase of bond cleavage energy due to the use of ethanol fuel	[75]
	Reports mainly on electrolyte engineering									
				NiO (40%) – $Gd_{0.1}Ce_{0.9}O_{1.95}$ (GDC) (40%) (1–2 mm)	$Gd_{0.1}Ce_{0.9}O_{1.95}$ (GDC) + MOH(M=Li,Na), MX_i (M=Li,Na,Ca,Sr, Ba; X=Cl,F; i = 1,2) Carbon 10 wt% $Ce_{0.8}Sm_{0.2}O_{1.5}$ (SDC)	$La_{0.6}Sr_{0.4}Co_{0.2}Fe_{0.8}O_{3-\delta}$ (LSCF)	330 at 600 °C 300 at 600 °C 213 at 500 °C 390 at 600 °C	2 M Methanol 1 M Ethanol	Ceria-salt composite ceramic electrolytes with high ionic conductivity and good chemical stability.	[59]
				Ni–Cu–ZnO composite $Ce_{0.8}Sm_{0.2}O_{1.5}$ (SDC) (1 mm)	Carbon 20 wt% $Ce_{0.8}Sm_{0.2}O_{1.5}$ (SDC)	Ni–Cu–ZnO + $Ce_{0.8}Sm_{0.2}O_{1.5}$ (SDC)	295 at 500 °C 516 at 600 °C	Methanol/water steam	Improvement of cell performance by superionic conduction of the composite electrolyte	[60]
					Carbon 25 wt% $Ce_{0.8}Sm_{0.2}O_{1.5}$ (SDC)		431 at 500 °C 603 at 600 °C			
					Carbon 30 wt% $Ce_{0.8}Sm_{0.2}O_{1.5}$ (SDC)		376 at 500 °C			

Table 2. continued

Main focus in anode studies: Coking	Kinetics	Stability	Anode	Electrolyte	Cathode	Maximum power density [mWcm^{-2}]	Fuel	Main points	Ref
Reports mainly on anode engineering									
			Pt(300 nm)	Yttria-doped barium zirconate (BYZ) (900 nm)	Pt(200 nm)	577 at 600 °C 5.6 at 250 °C	Methanol/ water vapor	Used highly ion-conductive BYZ and improved OCV by controlling the thickness and the pore size of BYZ layers	[69]
Reports mainly on cathode engineering					$Ba_{1-x}Sr_xCo_yFe_{1-y}O_{3-\delta}$ (BSCF)	200 at 500 °C 180 at 500 °C 200 at 500 °C	Methanol Ethanol		
			Cu–Ni, Cu–Ni–C (1 mm)	Ceria carbon composite (CCC)	$LaFe_{0.8}Ni_{0.2}O_3$ (LFN) (LaFeO-based)	500 °C 180 at 500 °C	Methanol Ethanol	Tri-metal oxide materials with good catalytic activity in direct operation of alcohol	[39]
					Tri-metal oxide (CuNiOx-ZnO)	300 at 500 °C 380 at 550 °C	Methanol		

commonly used material for anodes of alcohol-fueled LT-SOFCs. Ni has high electrical conductivity and excellent activity for hydrogen electrocatalytic oxidation. Particularly when used for the reforming of hydrocarbons and alcohols at temperatures near 500 °C, Ni shows a performance comparable with that of Pt group metals.[48–51] However, the Ni anode is vulnerable to coking because it accelerates the thermal decomposition of hydrocarbons, forming a significant amount of coke on the anode surface, which could cause a drastic decrease in performance when the SOFC is directly operated on alcohol fuel.[49] In order to solve the coking problem, many studies have reported on the use of Ni and Cu together as anode materials. Because Cu has poor catalytic cracking activity against hydrocarbons, carbon does not significantly deposit on the anode surface when Cu is used as an anode material.[52,53] Azimova et al. measured the performances of SOFCs with Ni–, Ni–Cu– (69/31 wt %), and Cu-based anodes using MeOH and EtOH as fuels. The anodes were prepared by infiltration of nickel acetate or copper acetate solutions. A higher amount of Cu inclusion decreased the anode performance owing to the inferior catalytic activity for fuel oxidation and the hydrocarbon reforming reaction of Cu compared to Ni, while mitigating the performance drop by preventing coking.[54]

Metal-oxide electrolyte composites that can maximize the density of a triple-phase boundary—the interface where electrolyte, electrode, and gas meet and electrochemical reactions preferentially occur—and prevent coking, have also been widely studied to improve anode kinetics. Composites of Ni/Cu and oxide-ion conducting oxides such as doped ceria (e.g., SDC and GDC), doped ceria-carbonate, and doped zirconia (e.g., YSZ) were mostly used as anodes, while composites of Ni and proton-conducting oxides such as Ni-$BaZr_{0.1}Ce_{0.7}Y_{0.1}Yb_{0.2}O_{3-\delta}$ (BZCYYb) and Ni-$BaZr_{0.1}Ce_{0.7}Y_{0.2}O_{3-\delta}$ (BZCY7) were also reported.[33,35,36,48,53–66] Liu et al. studied a MeOH-fueled SOFC with a NiO-SDC anode fabricated by pressing and precalcinating the mixed powders [Figure 3(a)].[55] In this work, a direct MeOH-fueled SOFC showed long-term stability without coking. High performances of the cells with Ni-ceria composite anodes clearly indicate the superior kinetic performance of the anodes. A report by Meng et al. demonstrated a cell with a Ni-SDC anode prepared by ball-milling, with a very thin electrolyte or uniform pore providing more active sites for fuel oxidation reactions.[57] Using MeOH as a fuel, high cell performances of 820, 520, 260, and 110 mW cm^{-2} at 600, 550, 500 and 450 °C, respectively, have been reported. Zhu et al. obtained cell performances of 330 and 300 mW cm^{-2} with MeOH and EtOH fuels, respectively, at 600 °C using Ni(40 %)-$Gd_{0.1}Ce_{0.9}O_{1.95}$(GDC) (40 %) as an anode prepared by sintering.[59] It should be noted, however, that even Ni-SDC ($Sm_{0.2}Ce_{0.8}O_{1.9}$) anodes have shown severe performance drops when operated with EtOH flames directly owing to carbon deposition.[56]

Additives such as carbon, carbonate, or other catalyst layers can further improve the anode performance. Feng et al.

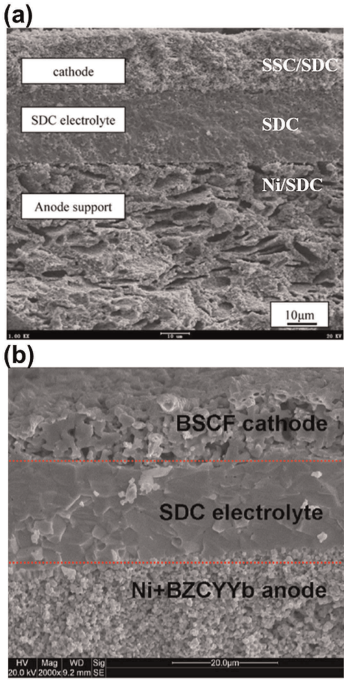

Figure 3. (a) Cross-sectional SEM image of the tested cell with Ni/SDC, SDC and SSC/SDC, and (b) typical SEM image of the fuel cells with a reduced Ni + BZCYYb anode. a) Reproduced with permission.[55] Copyright 2008, Elsevier. b) Reproduced with permission.[62] Copyright 2015, Elsevier.

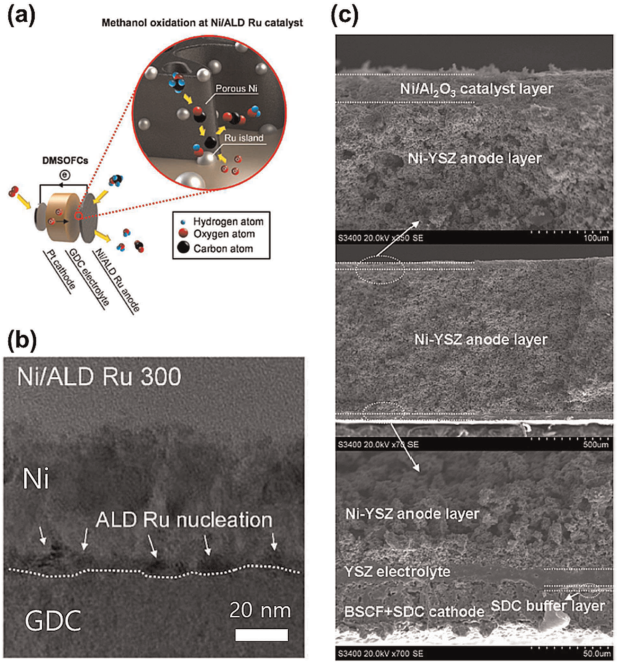

Figure 4. (a) Schematic of a direct methanol SOFC with a Ni/ALD Ru anode and the methanol oxidation process, (b) cross-sectional HR-TEM images of Ni/ALD Ru(300 cycles) microstructures, and (c) representative SEM images of a cross-section of a fuel cell with a reduced anode with a Ni/Al_2O_3 catalyst layer. a, b) Reproduced with permission.[49] Copyright 2016, American Chemical Society. c) Reproduced with permission.[48] Copyright 2014, Elsevier.

reported on a C–MO-SDC (C = activation carbon / carbon black, M = Cu, Ni, and Co, SDC = $Ce_{0.9}Sm_{0.1}O_{1.95}$) anode, which showed good performance owing to the high electronic conductivity of the anode by adding carbon.[58] Imran et al. used a composite anode of Ni–Cu-ZnO and SDC-Na_2CO_3 prepared by a solid-state reaction method, which led to a superior cell performance of 584 mW cm^{-2} at 570 °C. This confirmed that functional nanocomposite electrodes including carbonate are very effective for liquid-based fuel cells.[46] The addition of Pd to a NiO-YSZ cermet anode can enhance the cell performance, indicating that Pd facilitates the internal reforming/decomposition of MeOH at the anode.[61] The combined effects of high oxide-ion conductivity, small particle size, high water-storage capability, and good coking resistance of BZCYYb in a Ni-BZCYYb cermet anode also resulted in improved cell performance [Figure 3(b)].[62] The Ni/Al_2O_3 catalyst layer improved the EtOH steam reforming and showed high performance and good operational stability (> 100 h) [Figure 4(c)].[48] Similarly, the Ni + $Ce_{0.8}Zr_{0.2}O_2$ catalyst layer of a cermet anode improved anode kinetics as well as coking resistance.[65,66]

Studies with other kinds of Ni- and/or Cu-based composites have also been reported. Qin et al. used $Li_{0.2}Ni_{0.7}Cu_{0.1}O$ (NSDC) as an anode material with bioethanol and glycerol as fuels to study the effect of dipole moment responses of fuel molecules on the anode kinetics and coking resistance.[35,63,64] Jeong et al. fabricated an anode by depositing Ru on a porous Ni anode through atomic layer deposition (ALD) [Figures 4(a) and 4(b)].[49] In this study, a Ni anode coated with 300 cycles (~15 nm) of ALD Ru exhibited superior performance, which was over five times higher than that of a Ni-only anode because ALD Ru islands improved the surface kinetics for MeOH oxidation and coking resistance while stabilizing the porous Ni structure.

3.1.2. Noble Metal Based

Noble metal catalysts such as Pt, Pt–Ru alloy, Ag, or Pd can be used for anodes of alcohol-fueled LT-SOFCs. Bare Pt is recognized as the most effective catalyst for the deprotonation of alcohol molecules,.[67,68] Thus, several alcohol-fueled LT-SOFCs with Pt anodes have been reported. It is notable that a significant amount of CO is generated on the Pt catalyst surface when alcohol fuel is used for SOFCs with Pt anodes as opposed to when hydrogen fuel is used. In addition, the cell performance can also be significantly reduced because more complex reactions take place at the anode when alcohol fuel is used instead of hydrogen fuel. While most of the noble metal anodes were fabricated by sputtering techniques to make porous structures, there have been efforts to improve the morphology of the anode for better performance when integrated with other cell components. In a report from Ha et al., the use of a Pt layer (ALD Pt + sputtered Pt) for anodized aluminum oxide (AAO)-supported thin-film SOFCs was reported [Figure 5(a)].[69] The dense ALD Pt layer on the porous Pt anode effectively blocked the pores, which improved

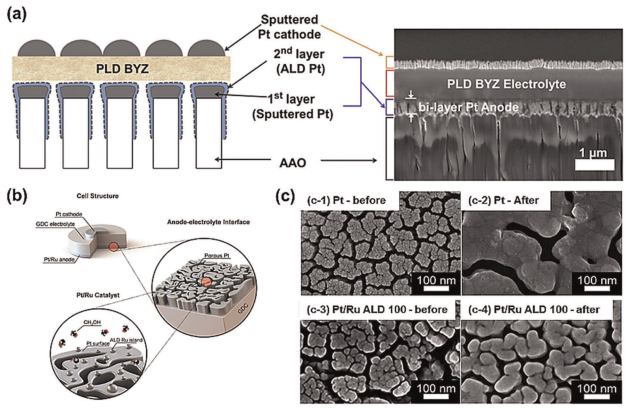

Figure 5. (a) SEM cross-sectional images of a BYZ fuel cell on AAO substrate (100 μm), Pt bi-layer anode (~300 nm), BYZ electrolyte (900 nm), and Pt anode (200 nm); (b) schematic of a GDC-based SOFC with porous Pt/Ru ALD anode; (c) FESEM images of (c-1)-(c-2) Pt, (c-3)-(c-4) Pt/Ru ALD 100, both before and after cell operation at 450 °C. a) Reproduced with permission.[69] Copyright 2013, Elsevier. b, c) Reproduced with permission.[71] Copyright 2015, American Chemical Society.

the density of the overlaying electrolyte, and resulted in a high OCV of ~0.8 V even with all thin-film components.

Ru added to a Pt anode can benefit anti-coking and the thermal stability of the anode. Komadina and Jeong used a Pt–Ru alloy as an anode to solve the possible issues associated with bare Pt anodes.[70–72] When Ru is added to the anode, hydroxyl groups are formed on the surface of the catalyst and effectively oxidize CO. Komadina et al., however, reported a very low cell performance ($<1\ mW\,cm^{-2}$) at 250–450 °C using MeOH fuel for the Pt–Ru anode prepared by sputtering because the catalytic activity of the Pt–Ru anode was significantly lower than that of the pure Pt anode.[70,73] On the other hand, Jeong et al. used a Pt–Ru anode, which was fabricated by the ALD coating of Ru on a porous Pt structure [Figures 5(b) and 5(c)].[71,72] The cell performance with the Ru-coated Pt anode improved by 5–10 times compared to that of a pure Pt anode with MeOH or EtOH fuel. The reason for such improvement was that the ALD Ru increases the surface kinetics and cell performance and oxidizes the CO adsorbed on the Pt surface. Furthermore, the passivating layer formed by Ru oxidation on the Pt surface suppresses the coarsening of the Pt cluster, leading to improved stability over prolonged operation.

To compensate the high price of a Pt-based anode, the use of Ag as the anode has also been reported. Poulianitis et al. compared the performance of Pt and Ag anodes with EtOH fuel, but the EtOH oxidation reaction on the surface of the Ag electrode turned out to be much slower than that on the surface of the Pt electrode.[74] Pd is also a possible alternative to replace Pt. Li et al. deposited a nanoporous Pd anode using sputtering, and then measured the performance using EtOH fuel.[75] Severe morphological degradation of the Pd anode, i.e., the spreading of Pd particles and droplet-like agglomeration of Pd, was observed with EtOH fuel possibly owing to the complexity of EtOH oxidation. However, no carbon deposition was detected on the Pd surface, which may imply a superior anti-coking characteristic of Pd compared to Pt.

3.2. Electrolyte

3.2.1. Oxide-Ion Conducting Ceramics

Fluorite oxides such as doped zirconia or doped ceria which contains doping induced oxygen ion vacancies are widely used as oxide ion-conducting electrolytes for LT-SOFCs. As in H_2-fueled LT-SOFCs, YSZ is one of the most widely used oxide-ion-conducting electrolyte materials in alcohol-fueled LT-SOFCs for its reasonably high ionic conductivity and superior thermal and mechanical properties. In addition, YSZ is chemically stable in both reducing and oxidizing conditions. Doped ceria materials such as GDC or SDC are also interesting electrolyte candidates for alcohol-fueled LT-SOFCs because of their higher ionic conductivity (approximately one order of magnitude higher than that of YSZ at 400–600 °C) and lower activation energy than that of YSZ, respectively, at a low-temperature region ($\leq$600 °C).[55–57,61] Electrolytes are usually fabricated as thin films with thicknesses of a few tens of micrometers or less to minimize the ohmic resistance.[48,53,65] They can be deposited using various techniques such as wet powder spraying,[48,53,65] particle suspension coating,[55] die-pressing,[56] co-firing,[57] tape-casting,[61] or co-precipitation.[77]

Composites consisting of ceria phase and salt phase have recently drawn much attention as novel electrolyte materials for alcohol-fueled LT-SOFCs. Their superior ionic conductivities effectively compensate the low cell performance due to slow anode kinetics by minimizing the ohmic loss. Gao et al. used a composite SDC electrolyte in their work; pure $Sm_{0.2}Ce_{0.8}O_{1.5}$ (SDC) powder was mixed with binary carbonates such as Li_2CO_3 and Na_2CO_3 (Figures 6(a) and 6(b)).[60,77] The SDC/Na_2CO_3 has more interacting fields between the two different phases because of their conformal distributions and smaller sizes. This structure is thought to provide higher conductivity and capacity for increasing the interfacial ion mobility compared to bulk mobility. For the similar reason, Imran investigated four different composite electrolytes with SDC and Na_2CO_3,[46] and Mat used ceria-salt composite electrolytes.[39]

3.2.2. Proton Conducting Ceramics

In order to sustain high ionic conductivity even at relatively low temperatures, the use of proton-conducting materials for SOFC electrolytes has been recently actively researched. Proton-conducting electrolytes conduct protons (H^+) instead of oxide-ions (O^{2-}). Since proton is relatively small compared to oxide ions, it possesses higher mobility, and therefore, higher ionic conductivity.[78–83] ABO_3-structured perovskite materials with protonic conductivity are usually used as proton-conducting electrolytes. Among the various ABO_3-

structured perovskite materials, doped barium zirconate ($BaZrO_3$) and doped barium cerate ($BaCeO_3$) have been widely investigated for electrolytes of LT-SOFCs. In particular, $BaZrO_3$ is more stable compared to $BaCeO_3$ in CO_2 environment in spite of its slightly lower proton conductivity than that of $BaCeO_3$, which is crucial in direct-alcohol fueled LT-SOFCs generating CO_2 in the operation. Further stability enhancement of $BaZrO_3$ could be achieved by yttria (Y_2O_3) doping.[84] $BaCeO_3$, in contrast, exhibits higher proton conductivity; however, its stability is relatively poor because of its decomposition into CeO_2 and $BaCO_3$ in CO_2 environment.[85–87] Compositional proton-conducting electrolyte with $BaZrO_3$ and $BaCeO_3$ has been recently introduced to enhance the performance of proton conducting fuel cells (PCFCs) operating at low temperatures.[88] Recent reports by Ha[69] and Li[75] demonstrated the use of dense thin film yttria-doped barium zirconate (BYZ, $BaZr_{0.8}Y_{0.2}O_{3-\delta}$) electrolyted by pulse laser deposition (PLD) technique for thin-film SOFCs (Figures 6(c) and 6(d)). The fabrication of relatively thick (30–35-μm) BCZYbCo electrolyte by casting followed by sintering for an alcohol-fueled PCFC was also reported.[54]

3.3. Cathode

Although most research studies on alcohol-fueled LT-SOFCs focus on the anode materials rather than on the cathode, the materials for the cathode should be also considered to obtain a reliable power output as well as thermal stability in a full-scale cell. The oxygen reduction reaction (ORR), which occurs at the cathode, is known to be the rate-determining step in low-temperature operations, and cathode polarization loss becomes significant in the operation of LT-SOFCs.[4,89]

Similar to conventional SOFCs that use hydrogen as a fuel,[90–92] the most widely employed cathode materials for alcohol-fueled SOFCs are doped perovskite ceramics. LSCF,[33] LSC,[54] and BSCF [Figure 7(a)][56,65] cathodes have been widely employed. Recently, interesting alternative cathode materials for alcohol-fueled LT-SOFCs have been reported. Mat et al. compared three different cathode materials: BSCF perovskite oxide, LaFeO-based perovskite oxide, and trimetal oxide. The $CuNiO_x$-ZnO cathode showed a peak power density of around 500 $mW\,cm^{-2}$ at 580 °C with methanol operation.[39] Similarly, $Li_{0.2}Ni_{0.7}Cu_{0.1}O$ composite with SDC has been used for a cathode.[35]

Noble metal cathode catalysts with higher catalytic activity for ORR than perovskite oxides at low temperatures have also been investigated. Several studies have reported the use of Pt or Ag as a cathode material for alcohol-fueled LT-SOFCs. Poulianitis et al. reported on the performance of Pt and Ag as both anode and cathode materials.[74] A Pt-based

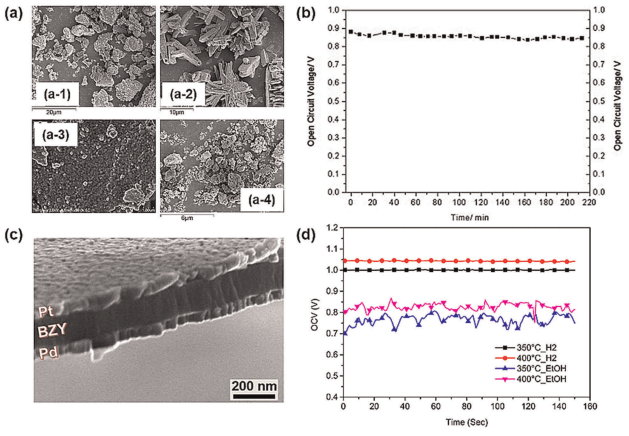

Figure 6. (a) SEM images of (a-1) Na_2CO_3, (a-2) SDC, (a-3) SDC/Na_2CO_3 nanocomposite, and (a-4) SDC-Na_2CO_3 microcomposite. (b) Long-term OCV stability of fuel cell driven by ethanol-water mixture solution of the cell with SDC/Na_2CO_3 composite electrolyte. (c) Cross-sectional image of Pt-BZY–Pd μ-SOFC structure after testing with H_2. (d) OCV evolution for dry H_2 and ethanol fuel testing at 350 and 400 °C. a,b) Reproduced with permission.[77] Copyright 2011, Elsevier. c,d) Reproduced with permission.[75] Copyright 2017, Elsevier.

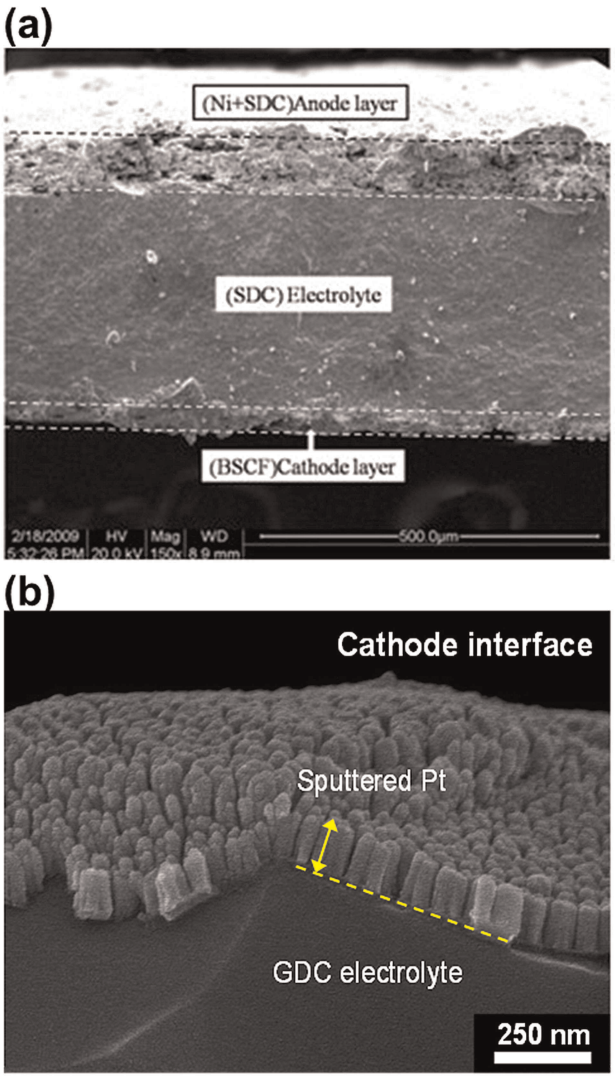

Figure 7. Cross-sectional SEM images of (a) BSCF cathode layer on SDC electrolyte-supported cell, (b) sputtered Pt cathode layer on GDC electrolyte-supported cell a) Reproduced with permission.[56] Copyright 2010, Elsevier. b) Reproduced with permission.[72] Copyright 2014, Elsevier.

cell showed a peak power density that was two times higher than that of an Ag-based cell at 550 °C. So far, the number of reports on the use of noble metal cathodes is relatively smaller than that of reports on the use of oxide-based cathodes because of their high cost (e.g., Pt: $30–$60/g) and low thermal stability owing to high surface energy.[93] Further investigations to enhance the thermal stability of noble metal electrodes are necessary, including Pt-based alloys with transition metals (e.g., Ni and Co)[94–96] and oxides(e.g., doped zirconia and doped ceria).[97–102] Novel composite cathodes such as core/shell nanofibers or nanospheres, which have been proven effective for H_2-fueled LT-SOFCs, could also be applied to alcohol-fueled LT-SOFCs.[103,104]

4. Electrochemical Performance

Figure 8 summarizes the power density results for alcohol-fueled LT-SOFCs, of which the maximum power densities

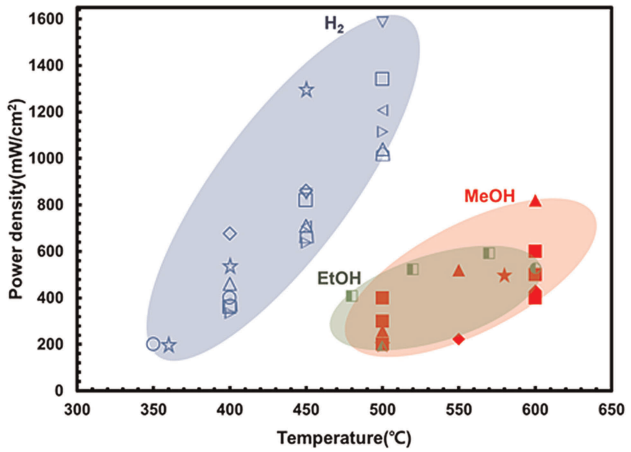

Figure 8. Summary of peak power densities of direct alcohol-fueled and H_2-fueled LT-SOFCs: MeOH-fueled(Gao(■),[60] Mat(■),[39] Liu(◆),[55] Meng(▲)[57]), EtOH-fueled(Imran(◧),[46] Wang(◐),[62] Mat(◭)[39]), and H_2-fueled(An(☆),[4] Chao(□),[9] Fan(△),[10] Huang(○),[7] Su(◇),[11] Lee(▽),[105] Li(◁),[19] Zhu(▷),[22] and Zhu(◯)[21]) LT-SOFCs.

exceed 200 mW cm^{-2} at operating temperatures of 600 °C and below. The power densities of H_2-fueled LT-SOFCs are presented for comparison. The power densities of alcohol-fueled SOFCs are generally even lower than those of H_2-fueled SOFCs owing to higher anodic activation loss. It has been reported that the concentration loss of EtOH-fueled SOFCs could be higher than that of MeOH-fueled ones owing to the larger molecular weight of EtOH.[53]

It will be insightful to summarize the actual MEA designs of high-performance alcohol-fueled LT-SOFCs. Reported high-performance alcohol-fueled LT-SOFCs are mostly based on anode-supported cell structures: the anodes are usually Ni- or Ni–Cu-electrolyte cermet composites, which can facilitate alcohol oxidation kinetics as well as anti-coking characteristics.[39,46,57,60] In terms of electrolytes, doped ceria materials are most widely used, but novel composites with improved ionic conductivity at low temperatures such as ceria + carbon [39] or ceria + carbonate[46,60] have drawn significant attention recently. Cathode materials widely used for H_2-fueled LT-SOFCs, e.g., BSCF[39,62] and LSCF,[57] have also been used in alcohol-fueled LT-SOFCs, while novel cathode materials such as $LaFe_{0.8}Ni_{0.2}O_3$ (LFN) or trimetal oxide have proven their superior activity at low temperatures.[39] Indeed, the MEA design by Gao (lithiated Ni–Cu-ZnO and electrolyte composites for anode/cathode and SDC + carbonate as electrolyte) is an example that demonstrates reasonably high OCV (0.8 V) with superior performance (431 mW cm^{-2} at 500 °C and 603 mW cm^{-2} at 600 °C with MeOH-water steam mixture).[60] The MEA reported by Meng (Ni-SDC(anode)/SDC(electrolyte) /SDC-LSCF(cathode) shows the highest performance at temperatures ≤ 600 °C (820 mW cm^{-2} at 600 °C).[57]

In summary, the best performance of a MeOH- or EtOH-fueled LT-SOFC (~ 430 mW cm^{-2} @ 500 °C)[60] is still significantly less than that of a H_2-fueled LT-SOFC (~ 1300 mW cm^{-2} @ 500 °C) at the same operating temperature.[9] Hence, more investigations on design and materials as well as operating conditions should be conducted to achieve higher performance, and thus, potentially wider applications of alcohol-fueled LT-SOFCs.

5. Commercialization

While the system based on alcohol-fueled LT-SOFCs does not yet seem to be released in the market, several commercial products of H_2-or hydrocarbon gas-fueled LT-SOFCs that could potentially share the same platform have been demonstrated for such applications as residential, transportation, and portable purposes. Redox Power Systems released a commercial product (25 kW) based on SOFC operating at low temperature (500–660 °6) with fuels including natural gas, propane, and biofuel for residential markets. Their systems obtain high power density (> 1 W cm^{-2}) even at this low temperature, and also are scalable for a broad range of power generation capacities due to modular nature (Figure 9(a)).[105] The SOFC system developed by Ceres Power also features a low temperature operation (500—620 °2) based on GDC electrolyte films; Ceres Power demonstrated a unique design of metal-supported type SOFC for 1 kW-class stack level system.[106] In the transportation sector, Nissan Motors recently announced the e-Bio Fuel-Cell prototype that employs SOFC stack to generate electricity to charge a battery for long range of > 600 km. Their prototype runs on 100-percent ethanol or ethanol-blended water, which means the zero-emission carbon-neutral driving (Figure 9(b)).[107] Low running costs, short refueling time as well as ample power supply of the e-Bio Fuel-Cell vehicle makes it ideal for wide range of customers. A couple of companies have demonstrated SOFC modules based on thin-film components. Lillipution Systems manufactured USB mobile power system based on LT-SOFC modules. The Si-based thin-film LT-SOFC of Lillipution's power system ran on butane fuel in

cartridge and generated the power of 2.5 W with the total energy of 55 Wh (Figure 9(c)).[108] SiEnergy Systems has demonstrated the macro-scale, thin-film SOFC based on micro-fabricated Si structures.[109] Their cells recorded the high power density of 155 mW cm^{-2} at 510 °t with the total power output of 20 mW per single SOFC chip, which is high enough for portable power.

6. Summary and Outlook

In this paper, recent results on membrane designs as well as materials and structures for individual components of LT-SOFCs directly operating with alcohol fuels have been reviewed. Electrochemical performances of direct MeOH- and EtOH-fueled LT-SOFCs have also been summarized and compared with those of H_2-fueled LT-SOFCs. Owing to high energy density as well as accessibility of liquid alcohols, LT-SOFCs directly operating with liquid alcohol can be attractive options as portable power sources.

Relatively low performance is one of the biggest challenges that direct alcohol-fueled LT-SOFCs have to overcome. While much effort has been made to lower the operating temperature of SOFCs to $\leq$600 °C, with some cells successfully demonstrating high performances with a power density of up to ~1.6 W cm^{-2} at temperatures as low as $\leq$500 °C with H_2 fuel,[4,9] alcohol-fueled LT-SOFCs still require extensive research in spite of their promising potentials. For instance, at an operating temperature of 600 °C, the best performance of direct MeOH-fueled LT-SOFC was 820 mW cm^{-2} reported by Meng et al.,[57] which is still lower than the performance requirement (>1 W cm^{-2}) for practical applications.

Novel combination of materials with nanoscale structures for components, i.e., anode, electrolyte, and cathode, is a promising research direction. As for electrolyte, thin-film electrolytes fabricated by various deposition techniques such as physical vapor deposition (PVD) or chemical vapor deposition (CVD) techniques can help reduce the ohmic resistance of the cells. Materials with exceptionally high ionic conductivities are also interesting for investigation: proton-conducting oxide, or bismuth oxide-based electrolytes doped or co-doped with various kinds of dopants have exhibited higher ionic conductivities than YSZ, GDC, or SDC did, which are widely used electrolyte materials. As for electrodes, highly catalytically active materials with nano-engineered structures are drawing much interest from researchers in the area of LT-SOFCs. For example, a recent report on H_2-fueled LT-SOFC observed a high catalytic activity for a cathode composed of a novel perovskite ($SrCo_{0.8}Nb_{0.1}Ta_{0.1}O_{3-\delta}$ (SCNT)) by the synergetic effect of two different dopants. Another recent study on H_2-fueled LT-SOFCs with exceptionally high performances (1.58 W cm^{-2} at 500 °C) made use of a nanostructured electrode such as a core-shell structured BSCF-GDC cathode with a nanocomposite anode functional layer (AFL).[105] Particularly in direct alcohol-fueled LT-SOFCs, anode catalyst is important. Thus, novel anode catalyst materials/structures should be developed to facilitate fuel oxidation with high coking resistance.

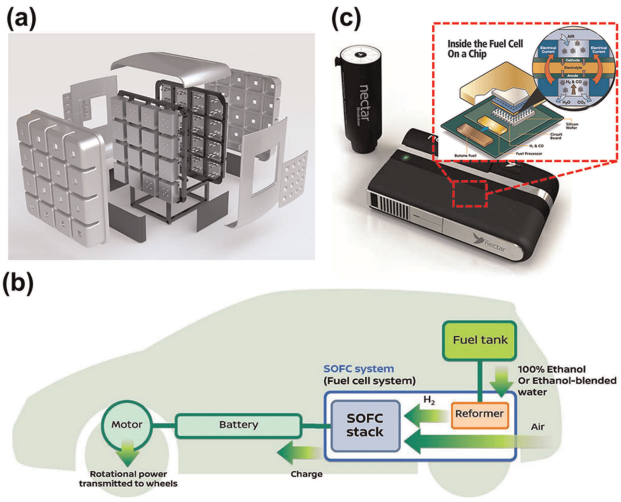

Figure 9. Examples of recent LT-SOFC based commercial products: (a) Redox Cube (25 kW) from Redox Power Systems,[105] (b) e-Bio Fuel Cell prototype from Nissan Motor,[107] and (c) portable battery charger from Lilliputian.[108]

It should also be noted that the nanoscale design of components should be carefully adopted in terms of stability as well as economics; together with the potentially poor mechanical strength of nanoscale structures, which often challenges large-scale production, the thermal stability could be a hurdle in employing nano-engineered components in alcohol-fueled LT-SOFCs. For example, electrodes containing metallic phase could be vulnerable to coarsening at elevated temperatures. Particularly at the anode, the morphology change can be even more severe due to complex oxidation processes. A thin-film electrolyte with nanoscale thickness could also suffer from structural as well as chemical instabilities. Moreover, process costs for nanoscale components such as thin films or nanofibers could also be higher than that of the conventional methods. Only with the careful design of materials, structures, and processes for cell components and membrane can make direct alcohol-fueled LT-SOFCs advance to the next stage from laboratory-level demonstration to system-level integration, and eventually, commercialization.

Abbreviations

AAO	Anodized aluminum oxide
AFL	Anode functional layer
ALD	Atomic layer deposition
ASR	Area specific resistance
BSCF	$Ba_{1-x}Sr_xCo_yFe_{1-y}O_{3-\delta}$
BYZ	Yttria-doped barium zirconate
BZCY7	$BaZr_{0.1}Ce_{0.7}Y_{0.2}O_{3-\delta}$
BZCYYb	$BaZr_{0.1}Ce_{0.7}Y_{0.1}Yb_{0.2}O_{3-\delta}$
CCC	Ceria carbon composite
CHP	Combined and power

CVD	Chemical vapor deposition
EtOH	Ethanol
GDC	Gadolinia-doped ceria
LPG	Liquefied petroleum gas
LSC	$La_{1-x}S_{rx}CoO_{3-\delta}$
LSCF	$La_{1-x}Sr_xCo_yFe_{1-y}O_{3-\delta}$
LT-SOFCs	Low temperature solide oxide fuel cells
MeOH	Methanol
OCV	Open circuit voltage
ORR	Oxygen reduction reaction
PCFCs	Proton conducting fuel cells
PLD	Pulse laser deposition
PVD	Physical vapor deposition
SCNT	$SrCo_{0.8}Nb_{0.1}Ta_{0.1}O_{3-\delta}$
SDC	Samaria-doped ceria
SOFCs	Solide oxide fuel cells
YSZ	Ytrria-stabilized zirconia
μ-SOFC	Micro Solide oxide fuel cells

Acknowledgements

J.A. acknowledges the financial support from National Research Foundation of Korea (NRF-2015R1D1 A1 A01058963 and NRF-2018R1C1 B6001150) and the Ministry of Trade, Industry and Energy (MOTIE), KOREA, through the Education Support program for Creative and Industrial Convergence (Grant Number: N0000717).

Conflict of interest

The authors declare no conflict of interest.

Keywords: Alcohols · Electrochemistry · Energy Conversion · Fuel Cells · Low-Temperature Solid Oxide Fuel Cell (LT-SOFC)

[1] B. C. Steele, A. Heinzel, *Nature* **2001**, *414*, 345–352.
[2] O. Yamamoto, *Electrochim. Acta* **2000**, *45*, 2423–2435.
[3] S. Park, J. M. Vohs, R. J. Gorte, *Nature* **2000**, *404*, 265–267.
[4] J. An, Y. B. Kim, J. Park, T. M. Gür, F. B. Prinz, *Nano Lett.* **2013**, *13*, 4551–4555.
[5] E. D. Wachsman, K. T. Lee, *Science* **2011**, *334*, 935–939.
[6] N. P. Brandon, S. Skinner, B. C. H. Steele, *Annu. Rev. Mater. Res.* **2003**, *33*, 183–213.
[7] H. Huang, M. Nakamura, P. Su, R. Fasching, Y. Saito, F. B. Prinz, *J. Electrochem. Soc.* **2007**, *154*, B20–B24.
[8] Y. B. Kim, T. M. Gür, S. Kang, H. J. Jung, R. Sinclair, F. B. Prinz, *Electrochem. Commun.* **2011**, *13*, 403–406.
[9] C.-C. Chao, C.-M. Hsu, Y. Cui, F. B. Prinz, *ACS Nano* **2011**, *5*, 5692–5696.
[10] Z. Fan, J. An, A. Iancu, F. B. Prinz, *J. Power Sources* **2012**, *218*, 187–191.
[11] P. C. Su, C. C. Chao, J. H. Shim, R. Fasching, F. B. Prinz, *Nano Lett.* **2008**, *8*, 2289–2292.
[12] M. Tsuchiya, B.-K. Lai, S. Ramanathan, *Nat. Nanotechnol.* **2011**, *6*, 282–286.
[13] J. D. Baek, C. C. Yu, P. C. Su, *Nano Lett.* **2016**, *16*, 2413–2417.
[14] Y. Zhang, R. Knibbe, J. Sunarso, Y. Zhong, W. Zhou, Z. Shao, Z. Zhu, *Adv. Mater.* **2017**, *1700132*.
[15] A. Evans, A. Bieberle-Hütter, J. L. M. Rupp, L. J. Gauckler, *J. Power Sources* **2009**, *194*, 119–129.
[16] S. Ji, J. Ha, T. Park, Y. Kim, B. Koo, Y. B. Kim, J. An, S. W. Cha, *Int. J. Precis. Eng. Manuf. - Green Technol.* **2016**, *3*, 35–39.
[17] T. Park, G. Y. Cho, Y. H. Lee, W. H. Tanveer, W. Yu, Y. Lee, Y. Kim, J. An, S. W. Cha, *Int. J. Hydrogen Energy* **2016**, *41*, 9638–9643.
[18] W. Yu, S. Ji, G. Y. Cho, S. Noh, W. H. Tanveer, J. An, S. W. Cha, *J. Vac. Sci. Technol.* **2015**, *33*, 01 A145.
[19] M. Li, M. Zhao, F. Li, W. Zhou, V. K. Peterson, X. Xu, Z. Shao, I. Gentle, Z. Zhu, *Nat. Commun.* **2017**, *8*, 13990.
[20] W. Zhou, J. Sunarso, M. Zhao, F. Liang, T. Klande, A. Feldhoff, *Angew. Chem. Int. Ed.* **2013**, *52*, 14036–14040; *Angew. Chem.* **2013**, *125*, 14286–14290.
[21] Y. Zhu, Z. G. Chen, W. Zhou, S. Jiang, J. Zou, Z. Shao, *ChemSusChem* **2013**, *6*, 2249–2254.
[22] Y. Zhu, W. Zhou, R. Ran, Y. Chen, Z. Shao, M. Liu, *Nano Lett.* **2016**, *16*, 512–518.
[23] S. Choi, S. Yoo, J. Kim, S. Park, A. Jun, S. Sengodan, J. Kim, J. Shin, H. Y. Jeong, Y. Choi, G. Kim, M. Liu, *Sci. Rep.* **2013**, *3*, 2426.
[24] S. Yoo, A. Jun, Y. W. Ju, D. Odkhuu, J. Hyodo, H. Y. Jeong, N. Park, J. Shin, T. Ishihara, G. Kim, *Angew. Chem. Int. Ed.* **2014**, *53*, 13064–13067; *Angew. Chem.* **2014**, *126*, 13280–13283.
[25] S. P. S. Badwal, S. Giddey, A. Kulkarni, J. Goel, S. Basu, *Appl. Energy* **2015**, *145*, 80–103.
[26] M. Cimenti, J. M. Hill, *Energies* **2009**, *2*, 377–410.
[27] D. Yue, S. Pandya, F. You, *Environ. Sci. Technol.* **2016**, *50*, 1501–1509.
[28] F. G. Ütu, S. M. Holmes, *Electrochim. Acta* **2011**, *56*, 8446–8456.
[29] F. Vigier, C. Coutanceau, A. Perrard, E. M. Belgsir, C. Lamy, *J. Appl. Electrochem.* **2004**, *34*, 439–446.
[30] M. Ni, D. Y. C. Leung, M. K. H. Leung, *Int. J. Hydrogen Energy* **2007**, *32*, 3238–3247.
[31] J. An, J. H. Shim, Y.-B. Kim, J. S. Park, W. Lee, T. M. Gür, F. B. Prinz, *MRS Bull.* **2014**, *39*, 798–804.
[32] M. Cimenti, J. M. Hill, *J. Power Sources* **2009**, *186*, 377–384.
[33] D. J. L. Brett, A. Atkinson, D. Cumming, E. Ramírez-Cabrera, R. Rudkin, N. P. Brandon, *Chem. Eng. Sci.* **2005**, *60*, 5649–5662.
[34] M. Mogensen, K. Kammer, *Annu. Rev. Mater. Res.* **2003**, *33*, 321–331.
[35] H. Qin, Z. Zhu, Q. Liu, Y. Jing, R. Raza, S. Imran, M. Singh, G. Abbas, B. Zhu, *Energy Environ. Sci.* **2011**, *4*, 1273.
[36] C. C. R. S. Rossi, C. G. Alonso, O. A. C. Antunes, R. Guirardello, L. Cardozo-Filho, *Int. J. Hydrogen Energy* **2009**, *34*, 323–332.
[37] T. Valliyappan, N. N. Bakhshi, A. K. Dalai, *Bioresour. Technol.* **2008**, *99*, 4476–4483.
[38] A. L. da Silva, I. L. Müller, *Int. J. Hydrogen Energy* **2010**, *35*, 5580–5593.
[39] M. D. Mat, X. Liu, Z. Zhu, B. Zhu, *Int. J. Hydrogen Energy* **2007**, *32*, 796–801.
[40] B. Zhu, X. Y. Bai, G. X. Chen, W. M. Yi, M. Bursell, *Int. J. Energy Res.* **2002**, *26*, 57–66.
[41] S. D. Nobrega, M. V. Galesco, K. Girona, D. Z. De Florio, M. C. Steil, S. Georges, F. C. Fonseca, *J. Power Sources* **2012**, *213*, 156–159.
[42] P. Vernoux, J. Guindet, M. Kleitz, *J. Electrochem. Soc.* **1998**.
[43] J.-M. Klein, S. Georges, Y. Bultel, *J. Electrochem. Soc.* **2008**, *155*, B333.
[44] J.-M. Klein, M. Hénault, P. Gélin, Y. Bultel, S. Georges, *Electrochem. Solid-State Lett.* **2008**, *11*, B144.
[45] J. M. Klein, M. Hénault, C. Roux, Y. Bultel, S. Georges, *J. Power Sources* **2009**, *193*, 331–337.
[46] S. K. Imran, R. Raza, G. Abbas, B. Zhu, *J. Fuel Cell Sci. Technol.* **2011**, *8*, 61014.
[47] J. H. Shim, S. Kang, S. W. Cha, W. Lee, Y. B. Kim, J. S. Park, T. M. Gür, F. B. Prinz, C. C. Chao, J. An, *J. Mater. Chem. A* **2013**, *1*, 12695–12705.
[48] W. Wang, F. Wang, R. Ran, H. J. Park, D. W. Jung, C. Kwak, Z. Shao, *J. Power Sources* **2014**, *265*, 20–29.
[49] H. Jeong, J. W. Kim, J. Park, J. An, T. Lee, F. B. Prinz, J. H. Shim, *ACS Appl. Mater. Interfaces* **2016**, *8*, 30090–30098.
[50] J. Rostrupnielsen, *J. Catal.* **1993**, *144*, 38–49.

[51] M. C. Sanchez-Sanchez, R. M. N. Yerga, D. I. Kondarides, X. E. Verykios, J. L. G. Fierro, *J. Phys. Chem. A* **2010**, *114*, 3873–3882.
[52] S. Park, R. Craciun, J. M. Vohs, R. J. Gorte, *J. Electrochem. Soc.* **1999**, *146*, 3603–3605.
[53] Y. Jiang, A. V. Virkar, *J. Electrochem. Soc.* **2001**, *148*, A706.
[54] M. A. Azimova, S. McIntosh, *J. Electrochem. Soc.* **2011**, *158*, B1532.
[55] M. Liu, R. Peng, D. Dong, J. Gao, X. Liu, G. Meng, *J. Power Sources* **2008**, *185*, 188–192.
[56] L. Sun, Y. Hao, C. Zhang, R. Ran, Z. Shao, *Int. J. Hydrogen Energy* **2010**, *35*, 7971–7981.
[57] X. Meng, Z. Zhan, X. Liu, H. Wu, S. Wang, T. Wen, *J. Power Sources* **2011**, *196*, 9961–9964.
[58] B. Feng, C. Y. Wang, B. Zhu, *Electrochem. Solid-State Lett.* **2006**, *9*, A80–A81.
[59] B. Zhu, *J. Power Sources* **2001**, *93*, 82–86.
[60] Z. Gao, R. Raza, B. Zhu, Z. Mao, *Int. J. Energy Res.* **2011**, *35*, 690–696.
[61] M. Sahibzada, B. C. H. Steele, K. Hellgardt, D. Barth, A. Effendi, D. Mantzavinos, I. S. Metcalfe, *Chem. Eng. Sci.* **2000**, *55*, 3077–3083.
[62] W. Wang, Y. Chen, F. Wang, M. O. Tade, Z. Shao, *Chem. Eng. Sci.* **2015**, *126*, 22–31.
[63] J. Y. Won, H. J. Sohn, R. H. Song, S. I. Woo, *ChemSusChem* **2009**, *2*, 1028–1031.
[64] N. Laosiripojana, S. Assabumrungrat, *J. Power Sources* **2007**, *163*, 943–951.
[65] W. Wang, C. Su, T. Zheng, M. Liao, Z. Shao, *Int. J. Hydrogen Energy* **2012**, *37*, 8603–8612.
[66] M. Liao, W. Wang, R. Ran, Z. Shao, *J. Power Sources* **2011**, *196*, 6177–6185.
[67] C. Lamy, A. Lima, V. LeRhun, F. Delime, C. Coutanceau, J. -M. Legér, *J. Power Sources* **2002**, *105*, 283–296.
[68] E. Antolini, *J. Power Sources* **2007**, *170*, 1–12.
[69] S. Ha, P.-C. Su, S. Ji, S. W. Cha, *Thin Solid Films* **2013**, *544*, 125–128.
[70] J. Komadina, Y. B. Kim, J. S. Park, T. M. Gür, S. Kang, F. B. Prinz, *ECS Trans.* **2011**, *35*, 2855–2866.
[71] H. J. Jeong, J. W. Kim, K. Bae, H. Jung, J. H. Shim, *ACS Catal.* **2015**, *5*, 1914–1921.
[72] H. J. Jeong, J. W. Kim, D. Y. Jang, J. H. Shim, *J. Power Sources* **2015**, *291*, 239–245.
[73] D. A. Stevens, J. M. Rouleau, R. E. Mar, A. Bonakdarpour, R. T. Atanasoski, A. K. Schmoeckel, M. K. Debe, J. R. Dahn, *J. Electrochem. Soc.* **2007**, *154*, B566.
[74] C. Poulianitis, V. Maragou, A. Y. Yan, S. Q. Song, P. Tsiakaras, *J. Fuel Cell Sci. Technol.* **2006**, *3*, 459–463.
[75] Y. Li, L. M. Wong, H. Xie, S. Wang, P. C. Su, *J. Power Sources* **2017**, *340*, 98–103.
[76] P. Li, B. Yu, J. Li, X. Yao, Y. Zhao, Y. Li, *Int. J. Hydrogen Energy* **2016**, *41*, 9059–9065.
[77] Z. Gao, R. Raza, B. Zhu, Z. Mao, C. Wang, Z. Liu, *Int. J. Hydrogen Energy* **2011**, *36*, 3984–3988.
[78] K. D. Kreuer, *Annu. Rev. Mater. Res.* **2003**, *33*, 333–359.
[79] K. Bae, D. Y. Jang, H. J. Choi, D. Kim, J. Hong, B.-K. Kim, J.-H. Lee, J.-W. Son, J. H. Shim, *Nat. Commun.* **2017**, *8*, 14553.
[80] H. Iwahara, H. Uchida, K. Ono, K. Ogaki, *J. Electrochem. Soc.* **1988**, *135*, 529–533.
[81] W. Münch, G. Seifert, K. D. Kreuer, J. Maier, *Solid State Ionics* **1997**, *97*, 39–44.
[82] T. Hibino, A. Hashimoto, M. Suzuki, M. Sano, *J. Electrochem. Soc.* **2002**, *149*, A1503.
[83] J. H. Shim, J. S. Park, J. An, T. M. Gür, S. Kang, F. B. Prinz, *Chem. Mater.* **2009**, *21*, 3290–3296.
[84] E. Fabbri, L. Bi, D. Pergolesi, E. Traversa, *Adv. Mater.* **2012**, *24*, 195–208.
[85] D. Shima, S. M. Haile, *Solid State Ionics* **1997**, *97*, 443–455.
[86] Z. L. Wu, M. L. Liu, *J. Electrochem. Soc.* **1997**, *144*, 2170–2175.
[87] G. Ma, *Solid State Ionics* **1998**, *110*, 103–110.
[88] K. Bae, S. Lee, D. Y. Jang, H. J. Kim, H. Lee, D. Shin, J. W. Son, J. H. Shim, *ACS Appl. Mater. Interfaces* **2016**, *8*, 9097–9103.
[89] H. S. Noh, K. J. Yoon, B. K. Kim, H. J. Je, H. W. Lee, J. H. Lee, J. W. Son, *J. Power Sources* **2014**, *247*, 105–111.
[90] S. Hou, J. A. Alonso, J. B. Goodenough, *J. Power Sources* **2010**, *195*, 280–284.
[91] D. Chen, C. Chen, F. Dong, Z. Shao, F. Ciucci, *J. Power Sources* **2014**, *250*, 188–195.
[92] Z. Cai, M. Kubicek, J. Fleig, B. Yildiz, *Chem. Mater.* **2012**, *24*, 1116–1127.
[93] J. An, Y.-B. Kim, F. B. Prinz, *Phys. Chem. Chem. Phys.* **2013**, *15*, 7520.
[94] N. M. Marković, T. J. Schmidt, V. Stamenković, P. N. Ross, *Fuel Cells* **2001**, *1*, 105–116.
[95] L. Xiong, A. Manthiram, *J. Electrochem. Soc.* **2005**, *152*, A697.
[96] H. A. Gasteiger, S. S. Kocha, B. Sompalli, F. T. Wagner, *Appl. Catal. B Environ.* **2005**, *56*, 9–35.
[97] H. J. Kim, J.-G. Yu, S. Hong, C. H. Park, Y.-B. Kim, J. An, *Phys. Status Solidi* **2017**, *1700465*, 1700465.
[98] Y. B. Kim, S. Hong, H. J. Kim, Y. B. Kim, J. An, *Ceram. Int.* **2017**, *43*, 5781–5788.
[99] K.-Y. Liu, L. Fan, C.-C. Yu, P.-C. Su, *Electrochem. Commun.* **2015**, *56*, 65–69.
[100] Y. H. Lee, G. Y. Cho, I. Chang, S. Ji, Y. B. Kim, S. W. Cha, *J. Power Sources* **2016**, *307*, 289–296.
[101] Y. K. Li, H. J. Choi, H. K. Kim, N. K. Chean, M. Kim, J. Koo, H. J. Jeong, D. Y. Jang, J. H. Shim, *J. Power Sources* **2015**, *295*, 175–181.
[102] I. Chang, S. Ji, J. Park, M. H. Lee, S. W. Cha, *Adv. Energy Mater.* **2015**, *5*, 1–7.
[103] V. D'Innocenzo, G. Grancini, M. J. P. Alcocer, A. R. S. Kandada, S. D. Stranks, M. M. Lee, G. Lanzani, H. J. Snaith, A. Petrozza, *Nat. Commun.* **2014**, *5*, 1–6.
[104] F. Liang, W. Zhou, Z. Zhu, *ChemElectroChem* **2014**, *1*, 1627–1631.
[105] "Solid Oxide Fuel Cell Development at Redox Power Systems, LLC": S. R. Bishop, L. Wang, T. Langdo and B. M. Blackburn, *The Electrochemical Society Conference*, **2017**.
[106] R. Leah, A. Bone, M. Lankin, A. Selcuk, R. Pierce, L. Rees, D. Corcoran, P. Muhl, C. Brackenbury, M. Selby, et al., *ECS Trans.* **2013**, *57*, 461–470.
[107] *Nissan unveils first Solid-Oxide Fuel Cell vehicle; fueled by ethanol, 600km range*, Green Car Congr. **2016**.
[108] C. Demerjian, *Lilliputian Systems makes a fuel cell on silicon wafers*, Semiaccurate **2013**, 5–7.
[109] S. Ramanathan, *Harvard, SiEnergy demo macro-scale, thin-film IT-SOFC*, Fuel Cells Bull. **2011**, *2011*, 10–11.
[110] J. G. Lee, J. H. Park, Y. G. Shul, *Nat. Commun.* **2015**, *5*, 1.

Manuscript received: October 19, 2017
Revised manuscript received: December 21, 2017
Accepted manuscript online: December 22, 2017
Version of record online: ■■, ■■

REVIEW

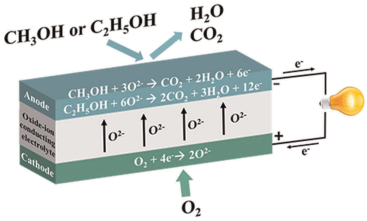

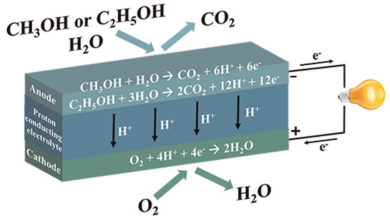

Low-temperature solid oxide fuel cells (LT-SOFCs, operating temperature $\leq 600\,^{\circ}C$) directly fueled with liquid alcohol are promising candidates for next-generation portable power sources. In this paper, recent results on direct alcohol-fueled LT-SOFCs are reviewed, focusing on materials, structures, and fabrication processes of the cell components. The electrochemical performances of alcohol-fueled LT-SOFCs are also reviewed and compared to those of H_2-fueled LT-SOFCs.

B. C. Yang, J. Koo, J. W. Shin, D. Go, Prof. J. H. Shim, Prof. J. An**

1 – 16

Direct Alcohol-Fueled Low-Temperature Solid Oxide Fuel Cells: A Review